Post-print of: Wachowski S., Mielewczyk-Gryń A., Gazda M.: Effect of isovalent substitution on microstructure and phase transition of LaNb1−xMxO4 (M=Sb, V or Ta; x=0.05–0.3). JOURNAL OF SOLID STATE CHEMISTRY. Vol. 219, (2014), p. 201-209. DOI: 10.1016/j.jssc.2014.07.041

Effect of isovalent substitution on microstructure and phase transition of $LaNb_{1-x}M_xO_4$ (M=Sb, V or Ta; x=0.05–0.3)

S. Wachowski [a] A. Mielewczyk-Gryn [a,b], M. Gazda [a]

[a] Faculty of Applied Physics and Mathematics, Department of Solid State Physics, Gdansk University of Technology, Narutowicza 11/12, 80-233 Gdansk, Poland
[b] Peter A. Rock Thermochemistry Laboratory and NEAT ORU, University of California, Davis, CA 95616, USA

a b s t r a c t

$LaNb_{1-x}M_xO_4$ oxides with pentavalent elements of different ionic sizes (M=Sb, Ta and V, x=0.05–0.3) were synthesized by the solid state reaction method. Special interest was devoted to the antimony substituted lanthanum niobate which is a new material in this group. Rietveld analysis of the X-ray diffraction patterns was used to determine the influence of the material composition on unit cell parameters. On the basis of dilatometric measurements phase transition temperatures and thermal expansion coefficients of the studied materials were determined. It was shown that with increasing concentration of Sb the phase transition temperature decreases. Thermal expansion coefficient of the antimony substituted samples above the transition temperature is in the range from 8.1 to 9.1 $\times 10^{-6}$ 1/K, whereas below the transition temperature the TEC value is between 14 and 17.3 $\times 10^{-6}$ 1/K. Influence of Ta, V and Sb substitutions on the microstructure and grain size was studied.

Keywords: Phase transition, Thermal expansion coefficient, Lanthanum niobate

1. Introduction

Functional ceramics and electroceramics, with their interesting electrical, magnetic, optical, thermal and other properties, have become one of the most important subjects of modern materials science. The performance of electroceramic materials depends on their structure, microstructure and high temperature properties. Many ceramic materials, e.g. ABO_4 (fergusonites, scheelites and wolframites), ABO_3 (perovskites) and AB_2O_4 (spinels) undergo structural phase transitions [1–4]. Since the structural phase transitions are important phenomena when it comes to analysis of the materials properties, the structural studies should be carried out. They include both high temperature and high pressure investigations. For instance, high pressure studies led to discovery of novel phases of strontium molybdate [5], characterization of the structural and electronic properties of various wolframites [6] and molibdates [7] and description of the mechanism of the phase transition in multiferroic $CuWO_4$ [8].

In this work the results of the structural and microstructural studies of lanthanum niobate, belonging to the ABO_4 group of oxides, substituted with the pentavalent elements on the niobium site, are reported and discussed. Special effort was devoted to the antimony substituted lanthanum niobate, $LaNb_{1-x}Sb_xO_4$ (x=0.05–0.3), which is a new material in this group. The aim of the studies was to determine the influence of antimony on the temperature of the phase transition. For comparison, also $LaNb_{1-x}Ta_xO_4$ and $LaNb_{1-x}V_xO_4$ (x=0.05–0.3) were studied.

Lanthanum niobates belong to a group of electroceramics technologically interesting for their proton conductivity [9]. Acceptor doped lanthanum niobates have been studied for the last ten years because of their relatively high ionic conductivity and stability in carbon dioxide containing atmospheres. At approximately 500 °C lanthanum niobate undergoes a transformation from the ferroeleastic phase with the monoclinic symmetry to the paraelastic tetragonal phase [1,2]. This leads to a thermal expansion coefficient (TEC) change which may worsen thermomechanical stability of material. The structural transformation also causes a change of the distances between the crystallographic planes between which hydrogen hopping occurs affecting the mobility of charge carriers. As a result the activation energy of conductivity is higher in the monoclinic phase than in the tetragonal one [10]. As a consequence, two strategies of the research concerning ABO_4 proton conductors have been carried out recently. One is to elaborate a material with the monoclinic fergusonite structure, stable up to high temperatures (e.g. 1000 °C) [11,12]. The other strategy is to stabilize the tetragonal scheelite structure in the whole temperature range above room temperature [13].

http://dx.doi.org/10.1016/j.jssc.2014.07.041

According to the literature data related to the ABO_4 materials a strong relation has been observed between the phase transition temperature and the ratio of the ionic radius of the cation to the ionic radius of the anion [11–16]. It was suggested that the stabilization of the tetragonal scheelite structure at low temperatures is most likely induced by the substitution of niobium with smaller isovalent cations [13]. Vanadium, tantalum and antimony are examples of elements which could be considered as isovalent substitutions. Niobium–oxygen polyhedra in $ANbO_4$ depend on the lattice symmetry. In the tetragonal structure, oxygen ions form a regular tetrahedron around Nb^{5+}; thus its coordination number is 4. On the other hand, in the monoclinic structure NbO_x polyhedra are often considered to be intermediate between isolated tetrahedra and edge-sharing chains of NbO_6 octahedra with two long Nb–O bonds [19,20]. Therefore, the coordination number of niobium in the monoclinic structure is considered as approaching 6. The ionic radius of Nb^{5+} with coordination number 4 is 0.48 Å, while that of V^{5+} is 0.36 Å [15]. In the case of coordination number 6 their ionic radii are 0.64 Å and 0.54 Å. It has been reported that a partial substitution of V^{5+} for Nb^{5+} leads to a decrease of the phase transition temperature [13]. On the other hand Ta^{5+} in lanthanum tantalate adopts octahedral coordination (coordination number=6) [22], which corresponds to ionic radius of 0.64 Å [21]. Therefore, introducing tantalum into lanthanum niobate causes the stabilization of the monoclinic structure [7,8]. Similarly to tantalum, Sb^{5+} in $ASbO_4$ and most other compounds assume coordination number equal to 6 [23,24]. Its ionic radius at the coordination number 6 is 0.62 Å [21]. Coordination number 4 is found in the compounds in which antimony is trivalent (with ionic radius 0.76 Å). Due to this it could be expected that the substitution with antimony should influence the phase transition temperature in the same way as the substitution with tantalum.

2. Experimental

2.1. Sample preparation

Samples of $LaNb_{1-x}M_xO_4$, where M=Ta, V and Sb and x=0.05–0.3, were prepared by the two-step solid state synthesis route. As starting reagents the La_2O_3 (Alfa-Aesar, Germany, 99.9% preheated at 900 °C), Nb_2O_5 (Alfa Aesar, Germany, 99.9985%) and one of the following V_2O_5 (Alfa Aesar, Germany, 99.9%), Ta_2O_5 (STREM, Germany, 99.8%) or Sb_2O_3 (POCH, Poland, 99%) were used. Stoichiometric amounts of the reagents were milled for 12 h using planetary ball mill. Then, the powders were uniaxially pressed into pellets under pressure of 180 MPa and calcined at 1200 °C for 8 h. Samples obtained in the first step were milled and pressed again into pellets under same conditions. The pellets were sintered at 1400 °C for 8 h. In order to prepare the samples for X-ray powder analysis the sintered samples were ground in an agate mortar.

2.2. Structural and microstructural characterization

Powder samples were examined by X-ray diffraction method using the Phillips X'Pert Pro MPD with Cu$K\alpha$1 and Cu$K\alpha$2 radiations. For high temperature measurements the samples were tested in the high temperature cell (Anthon Paar HT-XRD oven). The measurements were carried out between room temperature and 700 °C. In order to determine unit cell parameters the XRD patterns were analysed with Rietveld refinement method using the PANalytical HighScore Plus and FullProf Suite software. As an initial point of the analysis, unit cell parameters of the fergusonite (space group no. 15, $I2/c$) [20] and scheelite (space group no. 88, $I4_1/a$) [25] crystal structures of $LaNbO_4$ were utilized. Rietveld refinement was performed with the pseudo-Voigt profile function. The same function was applied for determination of the full width at half maximum of selected XRD reflections.

The relative length change of bulk samples was measured by Netzsch DIL 402 PC/4 dilatometer in argon ambient atmosphere in the temperature range 50–1000 °C with constant heating and with a constant cooling rate of 2 °C/min The temperature at which a change in slope of the dilatometric curve occurred was taken as the phase transition temperature. Thermal expansion coefficients below and above the transition temperature were calculated by fitting the relative elongation vs. temperature function with a linear function.

Micrographs of gold coated samples were obtained using FEI Quanta FEG 250 Scanning Electron Microscope with Everhart–Thorney detector in high vacuum mode. The analysis of the SEM images with the average grain intercept method was performed to obtain average grain size of the sintered materials. In each micrograph at least 15 random straight lines were drawn in order to determine the grain size. Averaged values from all lines were used for the average grain size of the current sample and a standard deviation was calculated as an average value uncertainty. Density of the samples was measured by the Archimedes method in ethanol. The relative density of the pressed and sintered pellets studied in this work was higher than 90%.

3. Results

3.1. Structural analysis

XRD patterns of $LaNb_{1-x}M_xO_4$, where M is Sb, V or Ta and x=0.05–0.3 collected at room temperature, are depicted in Fig. 1. All the reflections were indexed in either the monoclinic fergusonite-type structure ($I2/c$) or the tetragonal body-centred scheelite-type structure ($I4_1/a$). The widths of the main XRD reflections of monoclinic and tetragonal phases are collected in Table 1. It can be seen that Sb, V and Ta contents influence the reflection width in a different way. In the case of $LaNb_{1-x}Sb_xO_4$ the reflections are relatively narrow and their width does not depend on x. Increasing vanadium and tantalum causes either an increase or decrease of FWHM, respectively.

The XRD patterns were analysed with the Rietveld refinement method. Examples of the fitted profiles of the patterns recorded for $LaNb_{0.9}Sb_{0.1}O_4$ and $LaNb_{0.7}Sb_{0.3}O_4$, as well as the difference plots are shown in Fig. 2. The quality of the Rietveld profiles (R_p value) was between 12% and 18%. The patterns of materials substituted with either antimony or vanadium at concentrations lower than 25 mol% could be refined using monoclinic phase model. The samples containing 25 mol% of vanadium or 30 mol% of antimony were tetragonal, whereas in $LaNb_{0.75}Sb_{0.25}O_4$ both phases were present. In the case of Ta substitution all samples were monoclinic at room temperature. Unit cell parameters for $LaNb_{1-x}Sb_xO_4$, $LaNb_{1-x}V_xO_4$ and $LaNb_{1-x}Ta_xO_4$ are presented in Figs. 3–5, respectively. Evolution of unit cell parameters as a function of the antimony content in $LaNb_{1-x}Sb_xO_4$, presented in Fig. 3, shows that values of the a_m and c_m parameters of the monoclinic unit cell converge with increasing Sb content to the value of the a_t parameter of the tetragonal unit cell of $LaNb_{0.7}Sb_{0.3}O_4$. The monoclinic angle decreases with an increase of Sb concentration and reaches 90° for $LaNb_{0.7}Sb_{0.3}O_4$. A similar tendency can be seen in the case of vanadium substituted lanthanum niobate (Fig. 4). The vanadium content necessary for the stabilization of the tetragonal phase at room temperature (25 mol%) is lower than the antimony content (30 mol%). Tantalum concentration influence on the unit cell parameters is depicted in Fig. 5. It is visible that, in contrast to antimony and vanadium substituted samples, values of the a_m and c_m parameters diverge

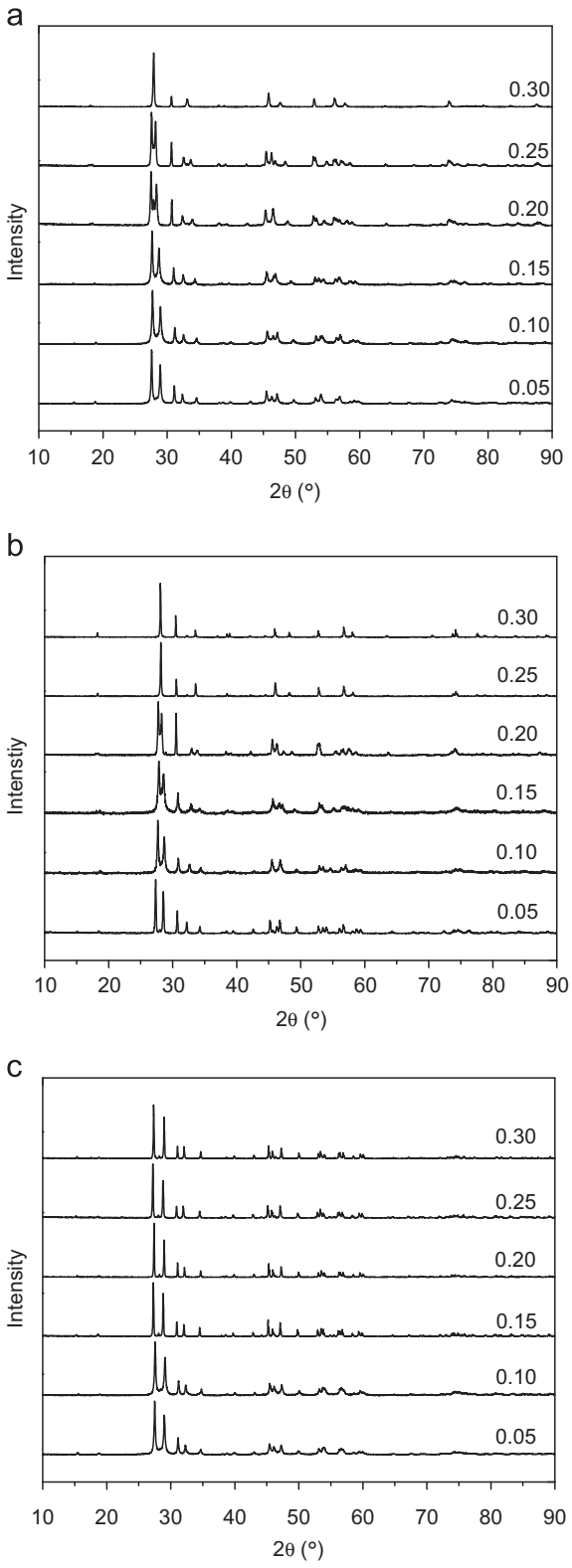

Fig. 1. Room temperature XRD diffractograms of lanthanum niobate substituted with (a) Sb, (b) V or (c) Ta.

while a value of monoclinic angle increases with increasing Ta concentration. Figs. 3–5 display also the evolution of unit cell volume with increasing content of Sb, V and Ta. It can be seen that the volume of unit cell monotonically increases with increasing amount of antimony whereas it decreases with increasing amount of tantalum. In the case of vanadium substituted samples, the unit

Table 1
Microstructural features of the $LaNb_{1-x}M_xO_4$ (M=Ta,V and Sb) samples. FWHM – full width at half maximum of the main XRD reflection (121) and (121) in monoclinic and tetragonal phases, respectively). FWHM of the (121) reflection corresponding to the tetragonal phase is marked with "*". D – average grain sizes estimated on the basis of SEM images of the samples sintered at 1400 °C for 8 h..

Element	Sb		V		Ta	
x	FWHM (°2θ)	D (μm)	FWHM (°2θ)	D (μm)	FWHM (°2θ)	D (μm)
0.05	0.19	1.6 ± 0.2	0.19	5 ± 1	0.20	1.5 ± 0.1
0.10	0.22	1.6 ± 0.2	0.14	7 ± 2	0.19	1.6 ± 0.2
0.15	0.23	1.9 ± 0.3	0.17	7 ± 2	0.15	1.8 ± 0.2
0.20	0.23	2.1 ± 0.3	0.27	7 ± 2	0.20	2.6 ± 0.5
0.25	0.21	2.7 ± 0.4	0.34	9 ± 2	0.10	7.4 ± 1.0
0.30	0.21*	2.8 ± 0.4	0.35	10 ± 2	0.10	7.8 ± 1.5

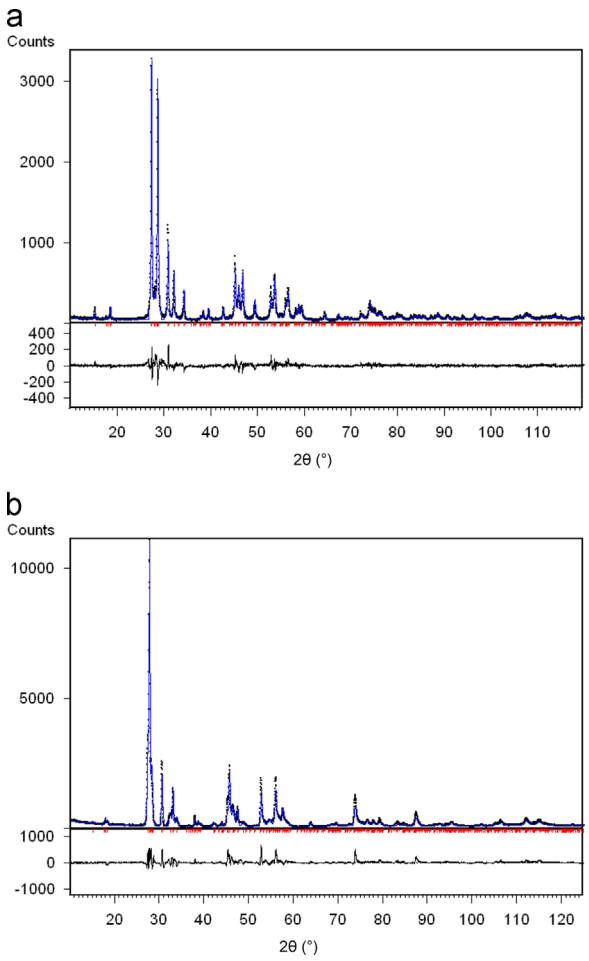

Fig. 2. Rietveld refinement patterns for (a) $LaNb_{0.9}Sb_{0.1}O_4$ and (b) $LaNb_{0.7}Sb_{0.3}O_4$ and the difference plots. Observed intensity data are shown by dots and the solid line is the calculated intensity.

cell volume of the monoclinic phase increases, while that of the tetragonal phase decreases with V content. Table 2 presents the atom coordinates of investigated compounds. In the case of samples with monoclinic structure niobium substitution does not affect the position of A- or B-site more than a few percent in relation to $LaNbO_4$. The substitution with Ta leads to an increase of the distance between A and B-site atoms, whereas Sb and V substitutions shorten this distance. Refining oxygen positions requires neutron diffraction data; however on the basis of the data shown in Table 2 it can be seen that the oxygen sites were

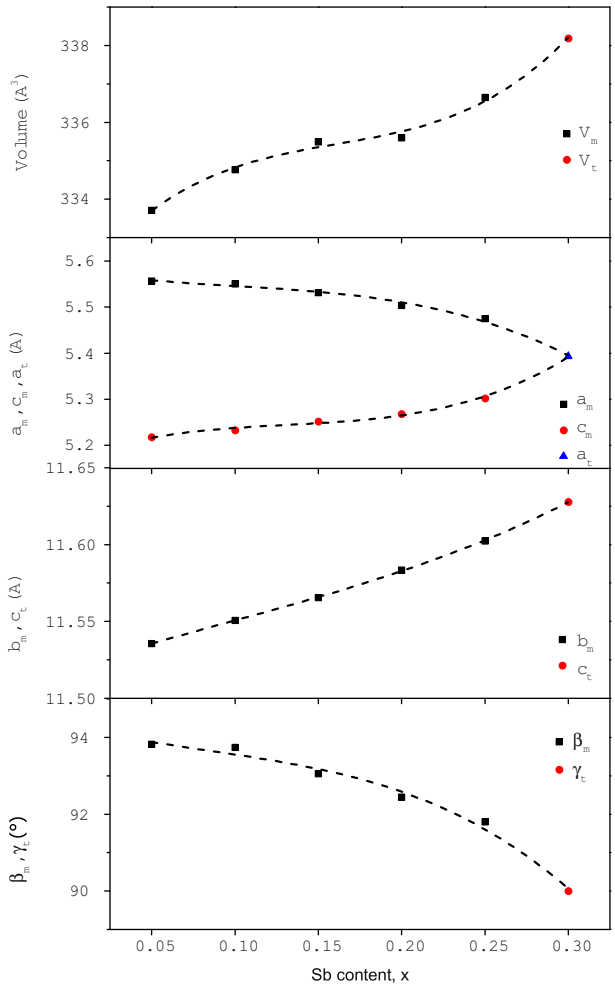

Fig. 3. Unit cell parameters and volume as a function of antimony content in the $LaNb_{1-x}Sb_xO_4$ samples (uncertainties are within the size of the points).

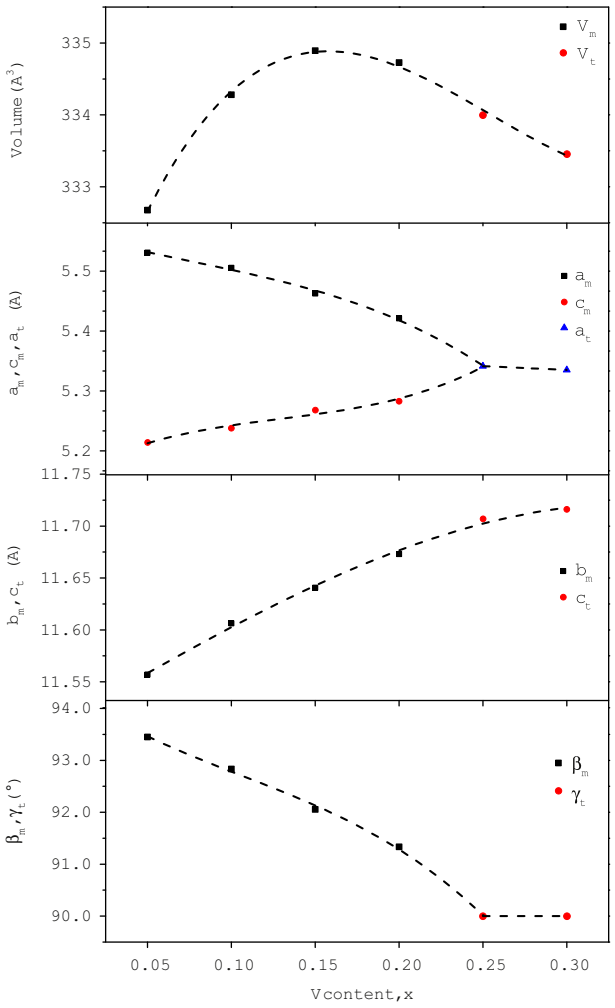

Fig. 4. Unit cell parameters and volume as a function of vanadium content in the $LaNb_{1-x}V_xO_4$ samples (uncertainties are within the size of the points).

altered more significantly, especially in the compound with tetragonal structure at room temperature. The difference in atom positions is bigger for antimony than vanadium substitution. The change of the oxygen site positions in compounds with tetragonal structure suggests the B–O bond length alteration and as result in change in the size of BO_4 tetrahedrons. This distortion is more visible for the material with antimony than those with vanadium.

The results of high temperature X-ray diffraction analysis carried out for the samples substituted with antimony are depicted in Fig. 6. The presented patterns are limited to the angle range in which main reflections characteristic of the monoclinic and tetragonal structures are present. In all patterns at low temperatures reflections characteristic of the monoclinic phase, $(\bar{1}21)$ and (130), are seen. In the pattern of $LaNb_{0.75}Sb_{0.25}O_4$, apart from them, a small reflection of the tetragonal phase, (121), is present at 50 °C. At higher temperature, the $(\bar{1}21)$ and (130), reflections of the monoclinic phase shift one towards another and finally merge into one (121) reflection of the tetragonal phase. It can be seen that a temperature range in which the structural transformation occurs decreases with the antimony content. In addition, unit cell parameters as a function of temperature are presented in Table 3. The reorientation of the unit cell during the phase transition from monoclinic fergusonite structure to tetragonal scheelite structure is reflected such that the values of *a* and *c* parameters of monoclinic structure approach the value of *a* parameter of tetragonal structure and *b* parameter of monoclinic structure and the value of parameter *c* of tetragonal one.

The results of dilatometric measurements of $LaNb_{1-x}Sb_xO_4$ materials are depicted in Fig. 7. Fig. 7 shows that for the sample with 30 mol% Sb a relative elongation increases linearly with temperature; thus the thermal expansion coefficient is constant in the studied temperature range. All other $LaNb_{1-x}Sb_xO_4$ samples revealed a change in slope of the temperature dependence of the elongation which signifies an abrupt change in thermal expansion coefficient associated with the phase transition from monoclinic to tetragonal structure. Linearity of the temperature dependence of the sample elongation in temperature ranges below and above the transition temperature allowed determining thermal expansion coefficients for the studied samples. Thermal expansion coefficients are presented in Table 4.

On the basis of the change in slope of the dilatometric curve the phase transition temperature was determined. Phase transition temperatures for samples containing Sb are shown in Table 4 and Fig. 8. It can be seen that the transition temperature decreases gradually with the antimony content.

3.2. *Microstructural analysis*

Scanning Electron Microscope micrographs of the surface of the studied samples are presented in Figs. 9–11. Average grain sizes estimated on the basis of SEM images analysis are collected in Table 1. SEM images of the surface of the antimony substituted samples are presented in Fig. 9. One can notice that the shape of

crystal grains is similar. There are no pores seen on the samples surface; however both inter- and intra-grain cracks may be seen. Fig. 9 also shows that the grains are larger in the sample containing more antimony. A trend of increasing average grain size with antimony concentration can be observed on the basis of data presented in Table 1. An average grain size increases from 1.6 μm (5 mol% of Sb) to 2.6 μm (30 mol% of Sb).

Microstructure of the surface of vanadium substituted lanthanum niobate is depicted in Fig. 10. Average grain size values are significantly larger than those of Sb and Ta substituted samples and the microstructure is different. In the vanadium substituted samples, apart from cracks, pores are also visible on the surface. Table 1 shows that grain size is increasing with the increasing concentration of vanadium.

The microstructure of tantalum substituted samples is presented in Fig. 11. Fig. 11a and b is representative of samples with lower (up to 20 mol%) and higher tantalum content (25 mol%), respectively. In either cases, no pores are seen on the samples surface, but inter- and intra-grain cracks are present. The grain sizes of the two shown samples are clearly different. As presented in Table 2 the average grain size of the samples with Ta concentrations of 25 mol% and 30 mol% is at least three times higher than that in the case of the samples with lower tantalum concentrations.

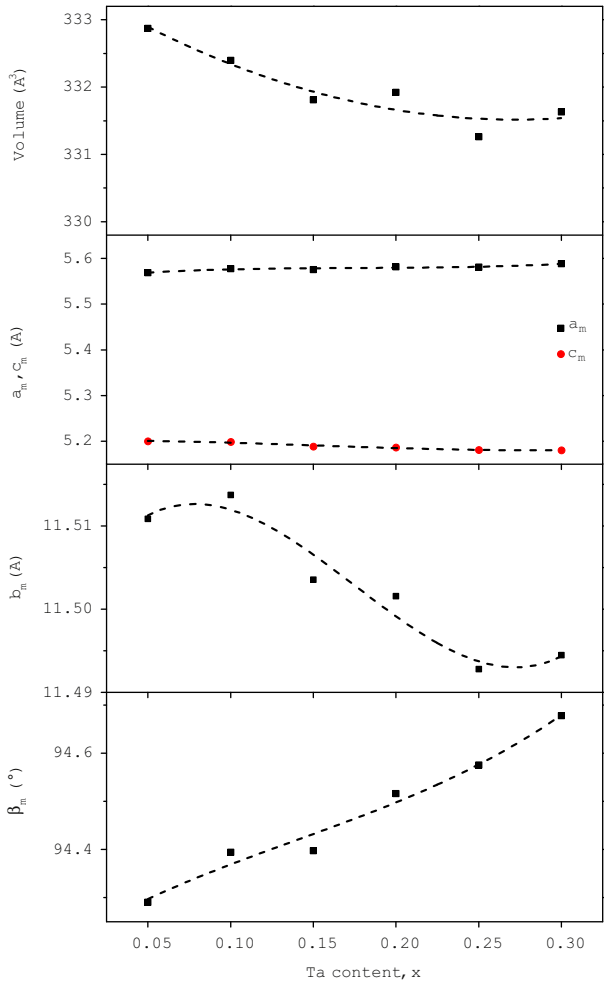

Fig. 5. Unit cell parameters and volume as a function of tantalum content in the $LaNb_{1-x}Ta_xO_4$ samples (uncertainties are within the size of the points).

4. Discussion

4.1. Structural analysis

The XRD analysis showed that antimony and vanadium substitutions stabilize the tetragonal structure whereas Ta stabilizes monoclinic phase. The influence of tantalum and vanadium substitutions on the crystal structure of lanthanum niobate is in a good agreement with previous studies [11–13]. These results are also consistent with a phase diagram describing the structure of ABO_4 compounds as related to the ionic radii ratios of cations and the anion, which was formulated first by Bastide [14] and further expanded by Errandonea and Manjón [15]. This phase diagram indicates that antimony, similar to tantalum substitution could be expected to stabilize the monoclinic fergusonite phase and increase the phase transition temperature. Our experimental results show that, in contrast to the above predictions, antimony stabilizes the tetragonal structure, which suggest that the ion size is not the only factor determining the structure of lanthanum niobates. It was assumed that antimony substitutes niobium as Sb^{5+}, not as Sb^{3+}. This assumption is based on the low solubility of acceptor substitutions in lanthanum niobate. The solubility of both *A*-site and *B*-site acceptors has been found lower than 1%, e.g. [17,18]. It has been postulated that low solubility of acceptor substitutions is caused by high energy of formation of extended defects related to oxygen vacancies [18]. To better understand why the influence of antimony on the lanthanum niobate structure is rather similar to that of vanadium instead of tantalum, it is necessary to analyse similarities and differences between these elements. Nb, V and Ta belong to group 5 of the periodic table while Sb to group 15. Therefore, the differences between

Table 2
Atom coordinates in crystal lattice of selected monoclinic and tetragonal compounds.

Compound	**$LaNb_{0.9}Sb_{0.1}O_4$**	**$LaNb_{0.7}Ta_{0.3}O_4$**	**$LaNbO_4$**[a]
Space group	*I*2/*c*	*I*2/*C*	*I*2/*C*
Atom; Wykoff symbol; *x*, *y*, *z*	La 4e 0, 0.6296(3), 0.25	La 4e 0, 0.6315(4), 0.25	La 4e 0, 0.6292(1), 0.25
	Nb 4e 0, 0.1054(2), 0.25	Nb 4e 0, 0.1014(3), 0.25	Nb 4e 0, 0.1036(1), 0.25
	Sb 4e 0, 0.1054(2), 0.25	Ta 4e 0, 0.1014(3), 0.25	–
	O1 8f 0.224(4), 0.038(1), 0.052(3)	O1 8f 0.243(5), 0.037(2), 0.043(5)	O1 8f 0.2376(2), 0.0337(1), 0.0546(2)
	O2 8f 0.170(2), 0.183(1), 0.459(2)	O2 8f 0.151(5), 0.205(2), 0.489(5)	O2 8f 0.1460(2), 0.2042(1), 0.4888(2)
Compound	**$LaNb_{0.7}Sb_{0.3}O_4$**	**$LaNb_{0.7}V_{0.3}O_4$**	**HT $LaNbO_4$**[b]
Space group	$I4_1/a$	$I4_1/a$	$I4_1/a$
Atom; Wykoff symbol; *x*, *y*, *z*	La 4b 0, 0.25, 0.625	La 4b 0, 0.25, 0.625	La 4b 0, 0.25, 0.625
	Nb 4a 0, 0.25, 0.125	Nb 4a 0, 0.25, 0.125	Nb 4a 0, 0.25, 0.125
	Sb 4a 0, 0.25, 0.125	V 4a 0, 0.25, 0.125	–
	O 16f 0.228(5), 0.091(3), 0.034(4)	O 16f 0.232(4), 0.103(3), 0.068(3)	O 16f 0.2441(5), 0.1599(3), 0.0850(3)

[a] Ref. [20].
[b] Ref. [25].

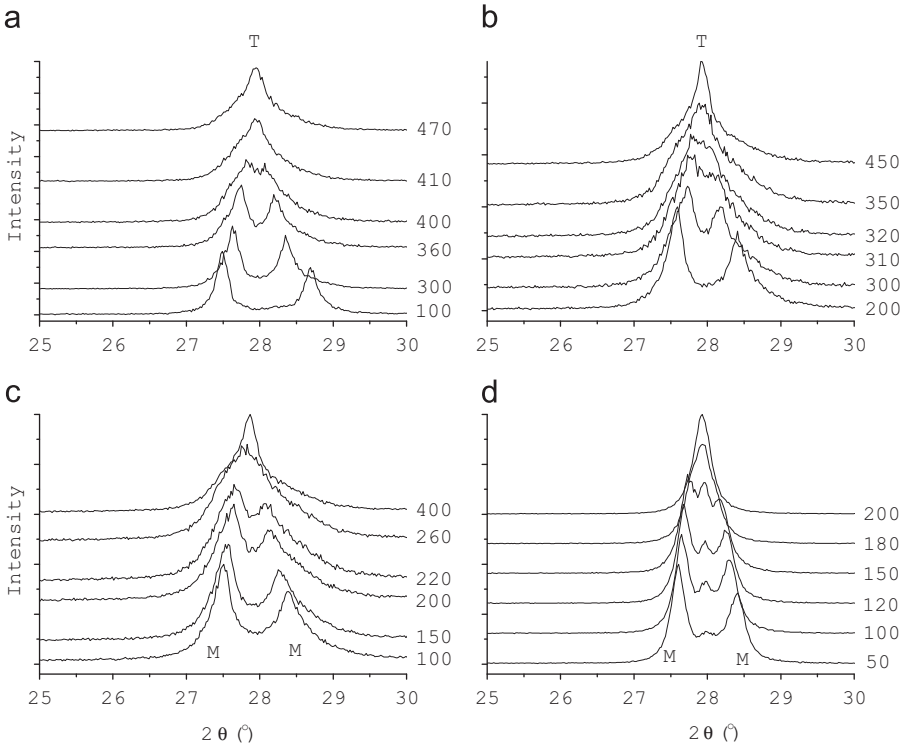

Fig. 6. XRD patterns at different temperatures for $LaNb_{1-x}Sb_xO_4$ samples: (a) $x=0.05$, (b) $x=0.10$, (c) $x=0.15$ and (d) $x=0.20$.

Table 3
Unit cell parameters as a function of temperature for selected $LaNb_{1-x}Sb_xO_4$ compounds.

T (°C)	a (Å)	b(Å)	c(Å)	β (deg)
$LaNb_{0.95}Sb_{0.05}O_4$, $T_0=404$ °C				
100	5.543(1)	11.552(2)	5.230(1)	93.483(2)
150	5.536(1)	11.568(2)	5.243(1)	93.214(6)
180	5.531(1)	11.578(2)	5.253(1)	93.038(7)
200	5.527(1)	11.586(2)	5.258(1)	92.917(7)
220	5.523(1)	11.593(2)	5.265(1)	92.781(7)
250	5.515(1)	11.603(2)	5.276(1)	92.577(8)
280	5.505(1)	11.611(2)	5.288(1)	92.341(8)
300	5.497(2)	11.616(2)	5.297(1)	92.167(8)
310	5.494(2)	11.617(3)	5.301(1)	92.068(8)
340	5.484(2)	11.628(3)	5.319(2)	91.790(10)
360	5.476(2)	11.641(3)	5.330(2)	91.536(11)
380	5.467(3)	11.645(5)	5.341(3)	91.358(15)
400	5.453(3)	11.645(5)	5.355(3)	91.027(15)
450	5.410(3)	–	11.659(6)	90
470	5.414(3)	–	11.657(5)	90
$LaNb_{0.85}Sb_{0.15}O_4$, $T_0=254$ °C				
50	5.524(1)	11.565(1)	5.258(1)	92.987(6)
100	5.516(1)	11.582(1)	5.274(1)	92.704(8)
150	5.505(1)	11.605(1)	5.298(1)	92.363(9)
200	5.487(1)	11.620(1)	5.319(1)	91.936(9)
220	5.490(2)	11.625(3)	5.332(2)	91.721(12)
260	5.403(1)	–	11.632(2)	90
290	5.403(1)	–	11.636(2)	90
340	5.406(1)	–	11.639(2)	90
400	5.405(1)	–	11.646(2)	90
$LaNb_{0.75}Sb_{0.25}O_4$, $T_0=125$ °C				
40	5.486(1)	11.596(2)	5.310(1)	91.993(7)
60	5.473(1)	11.594(2)	5.315(1)	91.747(7)
100	5.462(2)	11.618(2)	5.342(1)	91.337(13)
200	5.399(1)	–	11.618(2)	90
250	5.400(1)	–	11.628(1)	90
300	5.408(1)	–	11.635(1)	90
400	5.410(1)	–	11.658(2)	90

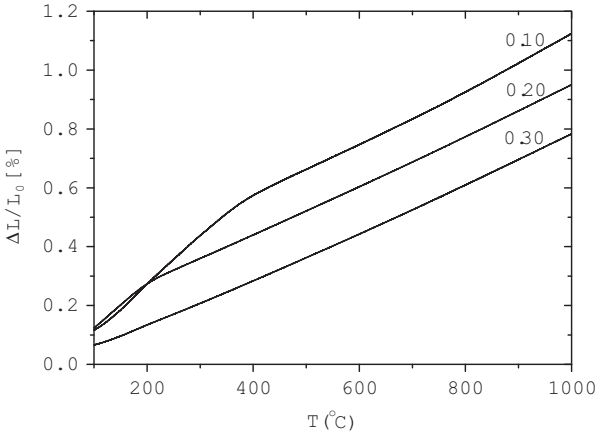

Fig. 7. Relative length change of the $LaNb_{1-x}Sb_xO_4$ samples as a function of temperature.

Table 4
Thermal expansion coefficients and transition temperatures of $LaNb_{1-x}Sb_xO_4$ samples.

x	Thermal expansion coefficient (10^{-6}/K) Structure		Transition temperature (°C)
	Monoclinic	Tetragonal	
0.05	16.2 ± 0.3	8.5 ± 0.3	404 ± 5
0.10	16.7 ± 0.4	9.1 ± 0.7	351 ± 5
0.15	17.3 ± 0.5	8.4 ± 0.3	254 ± 7
0.20	15.7 ± 1.2	8.3 ± 0.3	191 ± 9
0.25	14 ± 2	8.1 ± 0.4	125 ± 15
0.30	N/A	8.1 ± 0.3	$< RT$

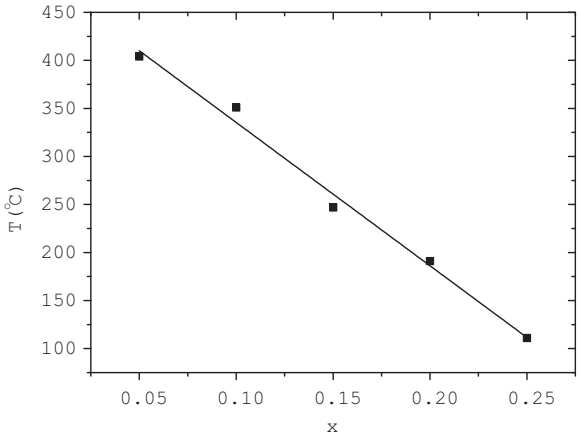

Fig. 8. Phase transition temperature of $LaNb_{1-x}Sb_xO_4$ as a function of Sb content.

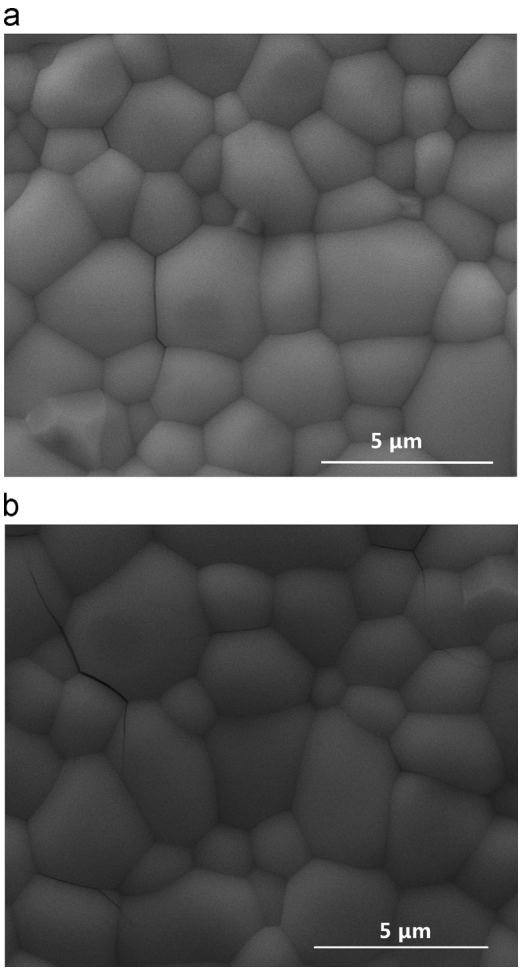

Fig. 9. SEM micrographs of the surface morphology for the $LaNb_{1-x}Sb_xO_4$ pellets with Sb content of (a) $x=0.15$ and (b) $x=0.3$.

electronegativities and electron configurations of the substituting elements and niobium should be taken into consideration.

The electronegativities of several elements in different valence states and coordination numbers have been recently quantitatively calculated on the basis of an effective ionic potential defined by the ionization energy and ionic radius by Li et al. [26]. Electronegativities of Nb^{5+}, Ta^{5+}, Sb^{5+} and V^{5+} are 1.862, 1.925, 1.971 and 2.03 [26], respectively. Bonds formed between oxygen and metal ions with higher values of electronegativity have stronger

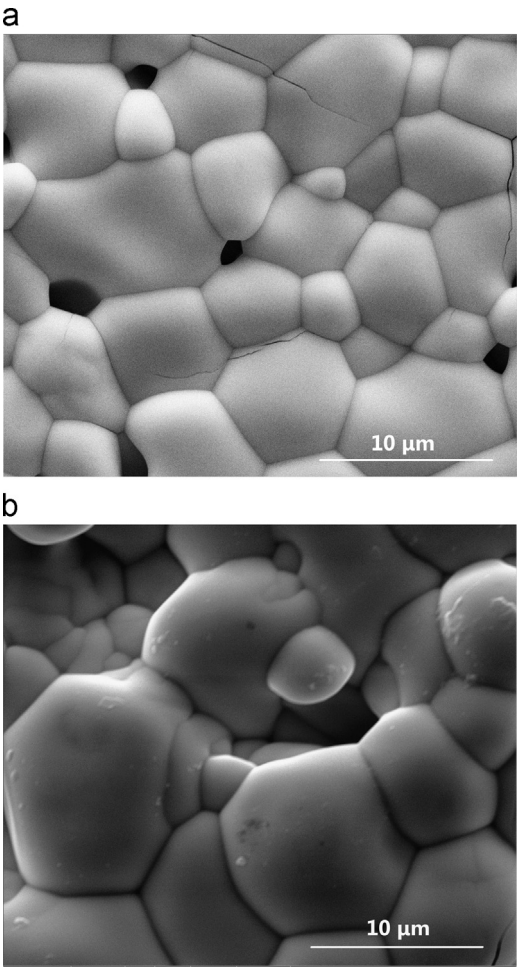

Fig. 10. SEM micrographs of the surface morphology for the $LaNb_{1-x}V_xO_4$ pellets with V content of (a) $x=0.15$ and (b) $x=0.3$.

ability to attract electrons from the oxide ions and are more covalent in comparison with bonds formed by oxygen and metal ions with lower electronegativity [27]. Covalency of bonds, in addition to the bond length, is an important factor influencing the structural properties of the studied compounds. Tsunekawa et al. found that the phase transition temperature of tantalates and niobates is correlated with the covalency of the Ta(Nb)–O bond which becomes the most shortened in the transition from monoclinic to tetragonal structure [20]. The difference between electronegativity of niobium and a substituting ion is the largest for vanadium (0.14), slightly smaller for antimony (0.11) and the smallest for tantalum (0.06). This indicates that an influence of the vanadium and antimony substitution on the bonds covalency may be considered as similar.

Electron configurations of Nb, V, Ta and Sb are [Kr] $4d^4\ 5s^1$, [Ar] $3d^3\ 4s^2$, [Xe] $4f^{14}\ 5d^3\ 6s^2$ and [Kr] $4d^{10}\ 5s^2\ 5p^3$, respectively. This means that the electron configuration of the Nb^{5+} and V^{5+} ions is similar to one another and corresponds to the closed shell of noble gas electronic configuration. However, Ta^{5+} electron configuration includes also 4*f* electrons, whereas Sb^{5+} electron configuration has 4*d* electrons. The influence of electron configuration of Nb^{5+} and Sb^{5+} on the symmetry of the double perovskite compounds of Ba_2LnSbO_6 and Ba_2LnNbO_6 (Ln – a lanthanide ion) was proposed by Saines et al. [28]. They suggested that since Nb^{5+} has empty orbitals, while Sb^{5+} occupied 4*d* orbitals, the 4*d* orbitals of the niobium ions are available to take part in π-bonding with the oxygen anions whereas the Sb 4*d* orbitals cannot. If π-bonding interactions affect the structural properties of lanthanum niobate

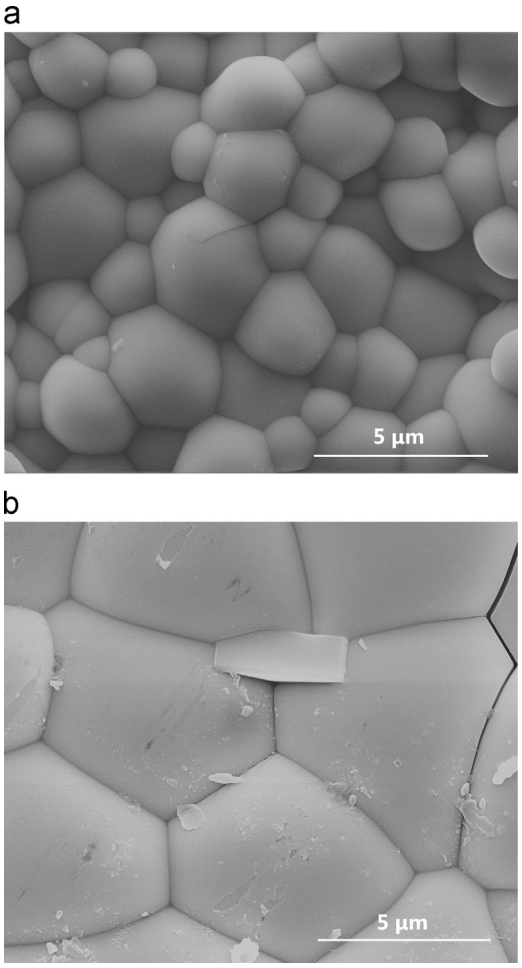

Fig. 11. SEM micrographs of the surface morphology for the $LaNb_{1-x}Ta_xO_4$ pellets with Ta content of (a) $x=0.15$ and (b) $x=0.3$.

substituted with vanadium, antimony and tantalum, it could be expected that $LaNb_{1-x}Sb_xO_4$ is similar to $LaNb_{1-x}Ta_xO_4$ while differs from $LaNb_{1-x}V_xO_4$. Since this is not the case, these differences between electron configurations between the substituting elements may be considered as weakly influencing structural properties of lanthanum niobates.

High temperature structural properties of $LaNb_{1-x}Sb_xO_4$ obtained with XRD and dilatometry methods support the room temperature structural analysis. As high-temperature XRD diffractograms (Fig. 6) and the results of dilatometric measurements show (Fig. 7, Table 2), the temperature in which the structural transformation occurs decreases with the antimony content. Lowering of the phase transition temperature with increasing content of Sb signifies the tetragonal structure stabilization by antimony substitution. The phase transition temperature tends to decrease linearly with Sb content (Fig. 8). As a result of structural studies it is confirmed that the solubility limit for the antimony substitution in lanthanum niobate has not been exceeded.

Apart from phase transition temperature, another important high temperature material property is the thermal expansion coefficient. TEC values obtained for $LaNb_{1-x}Sb_xO_4$ materials (between 8 and 9×10^{-6} 1/K or 16 and 17×10^{-6} 1/K in tetragonal or monoclinic phase, respectively) do not show, within the range of experimental uncertainties, a clear dependence on the antimony content. In general, they are similar to those reported for other compositions of lanthanum niobate. For example, thermal expansion coefficient value for pure lanthanum niobate [12] is 17.3×10^{-6} 1/K for monoclinic and 7.1×10^{-6} 1/K for tetragonal phase. It should be noted that the TEC of $LaNb_{0.7}Sb_{0.3}O_4$ is constant in the studied temperature range (8.1×10^{-6} 1/K). This is consistent with results reported by Brandão et al. [13] in $LaNb_{0.7}V_{0.3}O_4$ (8.0×10^{-6} 1/K). Slightly different thermal expansion coefficients, in comparison with other lanthanum niobates, were observed for $LaNb_{0.8}Ta_{0.2}O_4$, for which, TEC in the monoclinic and tetragonal structures was 15.7×10^{-6} 1/K and 9.1×10^{-6} 1/K, respectively [12]. Higher tanatalum content leads to further decrease of TEC. Tantalum, in contrast to vanadium- and antimony-substitution, leads to a decrease of unit cell volume. This may be related to stronger and less anharmonic bonds as well as a lower thermal expansion coefficient.

4.2. Microstructural analysis

Microstructural differences between the ceramics containing antimony, vanadium and tantalum (Figs. 9–11, Table 1) indicate that the processes of nucleation and growth depend on the characteristics of either these elements or their oxides and it is not a result of mechanical machining processes performed during material preparation. The ceramics were prepared in a two-step solid state synthesis and intermediate grinding and ball milling after the calcination at 1200 °C was applied. Ball milling process was able to deagglomerate the crystallites, but it was not energetic enough to crush them. Sintering at 1400 °C mainly lead to sample densification and possibly further growth of crystallites formed in the first step. Therefore it was assumed that the first step of the synthesis was crucial for the end material microstructure. Melting temperatures of the La_2O_3, Nb_2O_5, Sb_2O_3, V_2O_5 and Ta_2O_5 are 2315 °C, 1512 °C, 656 °C, 690 °C and 1872 °C, respectively [29–33]. This means that in the case of $LaNb_{1-x}Sb_xO_4$ and $LaNb_{1-x}V_xO_4$ the lanthanum niobate synthesis is assisted by a liquid phase formation. Since the presence of a liquid phase enhances diffusion, the grains' growth rate is expected to be higher in comparison to those related to the solid state diffusion only. It indicates the reason why the grains of $LaNb_{1-x}V_xO_4$ are larger than those of $LaNb_{1-x}Ta_xO_4$. During the synthesis of $LaNb_{1-x}Sb_xO_4$ compounds liquid phase should be present; therefore grain sizes similar to those of $LaNb_{1-x}V_xO_4$ could be expected. The lower average grain size of $LaNb_{1-x}Sb_xO_4$ may be partially caused by the necessity of the diffusion of oxygen from atmosphere related to the low valence state of antimony in Sb_2O_3. On the other hand, the oxidation of Sb_2O_3 has been reported to occur at about 530 °C [31]. Comparison of the XRD reflections width (Table 1) shows that the reflections of antimony substituted samples are narrow and their width does not depend on the antimony content. In the $LaNb_{1-x}V_xO_4$ samples reflections are also narrow for samples with $x<0.2$; however for samples with $x=0.2$ and 0.3 one may observe reflection widening. Narrow XRD reflections may be associated with a large crystallite size and the absence of residual strain. The broadening of the reflections of $LaNb_{1-x}V_xO_4$ for $x>0.2$ may be caused by the strain related to fact that in these samples phase transition temperature is close to the room temperature. The same effect could be expected in $LaNb_{1-x}Sb_xO_4$, but it appears to be much weaker.

The microstructure of tantalum substituted lanthanum niobate differs from the other studied materials. The bigger average grain size of $LaNb_{0.75}Ta_{0.25}O_4$ and $LaNb_{0.70}Ta_{0.30}O_4$, in comparison to $LaNb_{1-x}Ta_xO_4$ with $x\leq0.20$, suggests that high tantalum content significantly influences the solid state reaction. The studies of Nb_2O_5 and Ta_2O_5 bilayer formation reported by Cho et al. [34] indicated that the interdiffusion of Ta_2O_5 and Nb_2O_5 occurs even at temperature as low as 550 °C. Therefore, in the samples which consist of comparable amounts of niobium and tantalum oxides, the high rate of interdiffusion between them may significantly enhance the grain growth process.

5. Conclusions

The influence of antimony on the structural properties and the temperature of the phase transition of $LaNb_{1-x}Sb_xO_4$ was investigated and discussed. For comparison, also $LaNb_{1-x}V_xO_4$ and $LaNb_{1-x}Ta_xO_4$ were studied.

Unit cell parameters at room temperature of all studied compounds were determined. It has been presented that antimony, similar to vanadium substitution, tends to stabilize the tetragonal structure whereas Ta is a monoclinic phase promoter. The unit cells of $LaNb_{0.7}Sb_{0.3}O_4$ and $LaNb_{0.75}V_{0.25}O_4$ are tetragonal at room temperature.

Temperature of the structural transition from the monoclinic fergusonite to tetragonal scheelite structure for $LaNb_{1-x}Sb_xO_4$ was determined. The value of phase transition temperature decreases with increasing concentration of antimony. It has been shown that $LaNb_{0.7}Sb_{0.3}O_4$ sample does not undergo the phase transitions within the temperature range between room temperature and 1000 °C.

It has been found that the ionic radius, preferred coordination number and electronic configuration of antimony are similar to those of tantalum, whereas the electronegativity of Sb^{5+} is close to the electronegativity of vanadium. Therefore, it has been suggested that an influence of the vanadium and antimony substitution on the bonds covalency may be considered as a possible source of similar structural properties of $LaNb_{1-x}Sb_xO_4$ and $LaNb_{1-x}V_xO_4$.

Thermal expansion coefficients of $LaNb_{1-x}Sb_xO_4$ were determined. The TEC values for the tetragonal and monoclinic phases did not depend on the antimony content. In general, they were close to those reported for other compositions of the lanthanum niobate.

Microstructural analysis showed that the microstructure of the ceramics containing antimony, vanadium and tantalum differ. The interdiffusion of Ta_2O_5 and Nb_2O_5 has been proposed as the reason for unexpectedly large grains of $LaNb_{0.75}Ta_{0.25}O_4$ and $LaNb_{0.7}Ta_{0.3}O_4$.

References

[1] V.S. Stubican, J. Am. Ceram. Soc. 47 (1964) 55–58.
[2] A. Mielewczyk-Gryn, K. Gdula, T. Lendze, B. Kusz, M. Gazda, Cryst. Res. Technol. 45 (2010) 1225–1228.
[3] D. de Ligny, P. Richet, Phys. Rev. B 53 (1996) 3013–3022.
[4] C. Haas, J. Phys. Chem. Solids 26 (1965) 1225–1232.
[5] D. Errandonea, L. Gracia, R. Lacomba-Perales, A. Polian, J.C. Chervin, J. Appl. Phys. 113 (2013) 123510.
[6] J. Ruiz-Fuertes, S. Lòpez-Moreno, J. Lòpez-Solano, D. Errandonea, A. Segura, R. Lacomba-Perales, A. Muñoz, S. Radescu, P. Rodríguez-Hernández, M. Gospodinov, L.L. Nagornaya, C.Y. Tu, Phys. Rev. B 86 (2012) 125202.
[7] D. Errandonea, D. Santamaria-Perez, V. Grover, S.N. Achary, A.K. Tyagi, J. Appl. Phys. 108 (2010) 073518.
[8] J. Ruiz-Fuertes, A. Segura, F. Rodríguez, D. Errandonea, M.N. Sanz-Ortiz, Phys. Rev. Lett. 108 (2012) 166402.
[9] R. Haugsrud, T. Norby, Nat. Mater. 5 (2006) 193–196.
[10] H. Fjeld, K. Toyoura, R. Haugsrud, T. Norby, Phys. Chem. Chem. Phys. 12 (2010) 10313–10319.
[11] A.B. Santibáñez-Mendieta, E. Fabbri, S. Licoccia, E. Traversa, Solid State Ion. 216 (2012) 6–10.
[12] F. Vullum, F. Nitsche, S.M. Selbach, T. Grande, J Solid State Chem. 181 (2008) 2580–2585.
[13] A.D. Brandão, I. Antunes, J.R. Frade, J. Torre, V.V. Kharton, D.P. Fagg, Chem. Mater. 22 (2010) 6673–6683.
[14] J.P. Bastide, J. Solid State Chem. 71 (1987) 115–120.
[15] D. Errandonea, F.J. Manjón, Prog. Mater. Sci. 53 (2008) 711–713.
[16] F.J. Manjón, D. Errandonea, J. López-Solano, P. Rodríguez-Hernández, S. Radescu, A. Mujica, A. Muñoz, N. Garro, J. Pellicer-Porres, A. Segura, Ferrer-Roca Ch, R.S. Kumar, O. Tschauner, G. Aquilanti, Phys. Status Solidi B 244 (2007) 295–302.
[17] M. Huse, T. Norby, R. Haugsrud, Int. J. Hydrog. Energy 37 (2012) 8004–8016.
[18] M. Ivanova, S. Ricote, W.A. Meulenberg, R. Haugsrud, M. Ziegner, Solid State Ion. 213 (2013) 45–52.
[19] E. Papulovskiy, A.A. Shubin, V.V. Terskikh, C.J. Pickard, O.B. Lapina, Phys. Chem. Chem. Phys. 15 (2013) 5115–5131.
[20] S. Tsunekawa, T. Kamiyama, K. Sasaki, H. Asano, T. Fukuda, Acta Crystallogr. A49 (1993) 595–600.
[21] R.D. Shannon, Acta Crystallogr. A32 (1976) 751–767.
[22] M. Machida, S. Murakami, T. Kijima, S. Matsushima, W. Arai, J. Phys. Chem. B 105 (2001) 3289–3294.
[23] C. Hirschle, J. Rosstauscher, C. Rohr, Acta Crystallogr. C57 (2001) 1239–1241.
[24] K.P.F. Siqueira, R.M. Borges, J.C. Soares, A. Dias, Mater. Chem. Phys. 140 (2013) 255–259.
[25] W.I.F. David, Mater. Res. Bull. 18 (1983) 749–756.
[26] K. Li, D. Xue, J. Phys. Chem. A 110 (2006) 11332–11337.
[27] V. Dimitrova, T. Komatsu, J. Solid State Chem. 196 (2012) 574–578.
[28] P.J. Saines, B.J. Kennedy, M.M. Elcombe, J. Solid State Chem. 180 (2007) 401–409.
[29] S.G. Tresvyatskii, L.M. Lopato, Sov. Powder Metall. Met. Ceram. 2 (1963) 366–369.
[30] R.L. Orr, J. Am. Chem. Soc. 75 (1953) 2808–2809.
[31] R.G. Orman, D. Holland, J. Solid State Chem. 170 (2007) 2587–2596.
[32] F. Holtzberg, A. Reisman, M. Berry, M. Berkenblit, J. Am. Chem. Soc. 78 (1956) 1536–1540.
[33] A. Reisman, F. Holtzberg, M. Berkenbelt, M. Berr, J. Am. Chem. Soc. 78 (1956) 4514–4520.
[34] K. Cho, J. Lee, J.S. Lim, H. Lim, J. Lee, S. Park, et al., Microelectron. Eng. 80 (2005) 317–320.